Article

To Dope Mn in a Semiconducting Nanocrystal

Angshuman Nag, S. Chakraborty, and D. D. Sarma

J. Am. Chem. Soc., **2008**, 130 (32), 10605-10611 • DOI: 10.1021/ja801249z • Publication Date (Web): 19 July 2008

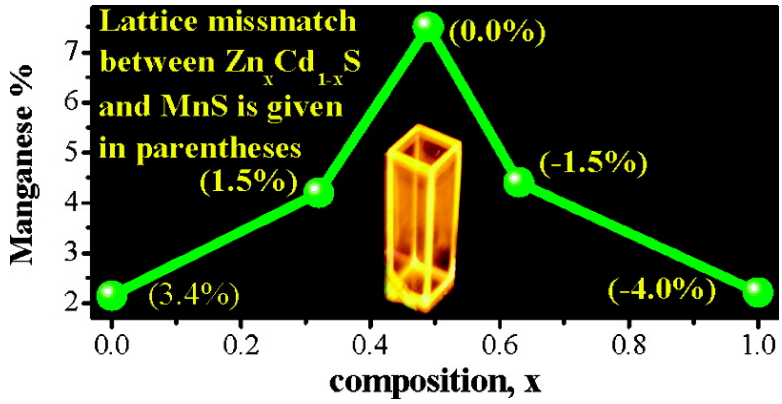

More About This Article

Additional resources and features associated with this article are available within the HTML version:

- Supporting Information
- Links to the 1 articles that cite this article, as of the time of this article download
- Access to high resolution figures
- Links to articles and content related to this article
- Copyright permission to reproduce figures and/or text from this article

View the Full Text HTML

J|A|C|S
ARTICLES

Published on Web 07/19/2008

To Dope Mn^{2+} in a Semiconducting Nanocrystal

Angshuman Nag,[†] S. Chakraborty,[‡] and D. D. Sarma*[,†,‡,§]

Solid State and Structural Chemistry Unit, Indian Institute of Science, Bangalore-560 012, India and Centre for Advanced Materials, Indian Association for the Cultivation of Science, Kolkata-700032, India

Received February 20, 2008; E-mail: mlsdds@iacs.res.in

Abstract: It has been an outstanding problem that a semiconducting host in the bulk form can be doped to a large extent, while the same host in the nanocrystal form is found to resist any appreciable level of doping rather stubbornly, this problem being more acute in the wurtzite form compared to the zinc blende one. In contrast, our results based on the lattice parameter tuning in a $Zn_xCd_{1-x}S$ alloy nanocrystal system achieves ~7.5% Mn^{2+} doping in a *wurtzite* nanocrystal, such a concentration being substantially higher compared to earlier reports even for nanocrystal hosts with the "favorable" zinc-blende structure. These results prove a consequence of local strains due to a size mismatch between the dopant and the host that can be avoided by optimizing the composition of the alloyed host. Additionally, the present approach opens up a new route to dope such nanocrystals to a macroscopic extent as required for many applications. Photophysical studies show that the quantum efficiency per Mn^{2+} ion decreases exponentially with the average number of Mn^{2+} ions per nanocrystal; en route, a high quantum efficiency of ~25% is achieved for a range of compositions.

Introduction

Introducing impurity ions into a semiconducting host to change its properties, termed doping, has been one of the most important techniques that paved the way for the modern technology of the twentieth century based on semiconducting devices. sp-d exchange interaction between paramagnetic dopant ions and semiconductor charge carriers in a bulk dilute magnetic semiconductor (DMS) gives rise to numerous remarkable magnetic and magnetooptical properties.[1,2] Another route to derive new properties has been to fashion a semiconductor in nanometer-sized entities because of their uniquely tunable properties arising from the quantum confinement of excited electron−hole pairs by the crystallite boundary.[3–10] With the hope of combining unique advantages of quantum confinement with those of DMS,[11] a huge interest[12–26] has developed in recent times to study the DMS NCs (nanocrystals). Manganese with its sharp, atomic-like emission line in the visible range has been the dominant choice for the dopant ion, while group II−VI semiconductors are popular for simplicity of synthesis and ease of size control. While doping in trace quantities is often sufficient for various electronic devices, many recent technologies as well as future ones are based on a larger extent of doping to derive properties beyond the electronic ones, such as optical, optoeletronic (converting light into energy[27]), and magnetic properties.[1,2] For example, it is shown that the ferromagnetic curie temperature (T_C) tends to increase with an increase in the concentration of transition metal ions in DMS

[†] Indian Institute of Science.
[‡] Indian Association for the Cultivation of Science.
[§] Also at Jawaharlal Nehru Centre for Advanced Scientific Research, Bangalore 560054, India.

(1) Ohno, H. *Science* **1998**, *281*, 951.
(2) Das Sarma, S. *American Scientist* **2001**, *89*, 516.
(3) Nirmal, M.; Brus, L. *Acc. Chem. Res.* **1999**, *32*, 407.
(4) Nanda, J.; Sapra, S.; Sarma, D. D.; Chandrasekharan, N.; Hodes, G. *Chem. Mater.* **2000**, *12*, 1018.
(5) Sapra, S.; Sarma, D. D. *Phys. Rev. B* **2004**, *69*, 125304.
(6) Talapin, D. V.; Shevchenko, E. V.; Murray, C. B.; Kornowski, A.; Foerster, S.; Weller, H. *J. Am. Chem. Soc.* **2004**, *126*, 12984.
(7) Viswanatha, R.; Sarma, D. D. *Chem.—Eur. J.* **2006**, *12*, 180.
(8) Robel, I.; Kuno, M.; Kamat, P. V. *J. Am. Chem. Soc.* **2007**, *129*, 4136.
(9) Viswanatha, R.; Amenitsch, H.; Sarma, D. D. *J. Am. Chem. Soc.* **2007**, *129*, 4470.
(10) Viswanatha, R.; Santra, P. K.; Dasgupta, C.; Sarma, D. D. *Phys. Rev. Lett.* **2007**, *98*, 255501.
(11) Sapra, S.; Sarma, D. D.; Sanvito, S.; Hil, N. A. *Nano Lett.* **2002**, *2*, 605.
(12) Levy, L.; Feltin, N.; Ingert, D.; Pileni, M. P. *J. Phys. Chem. B* **1997**, *101*, 9153.
(13) Stowell, C. A.; Wiacek, R. J.; Saunders, A. E.; Korgel, B. A. *Nano Lett.* **2003**, *3*, 1441.
(14) Sapra, S.; Prakash, A.; Ghangrekar, A.; Periasamy, N.; Sarma, D. D. *J. Phys. Chem. B* **2005**, *109*, 1663.
(15) Pradhan, N.; Goorskey, D.; Thessing, J.; Peng, X. *J. Am. Chem. Soc.* **2005**, *127*, 17586.
(16) Erwin, S. C.; Zu, L.; Haftel, M. I.; Efros, A. L.; Kennedy, T. A.; Norris, D. J. *Nature* **2005**, *436*, 91.
(17) Dalpian, G. M.; Chelikowsky, J. R. *Phys. Rev. Lett.* **2006**, *96*, 226802.
(18) Zu, L.; Norris, D. J.; Kennedy, T. A.; Erwin, S. C.; Efros, A. L. *Nano Lett.* **2006**, *6*, 334.
(19) Viswanatha, R.; Chakraborty, S.; Basu, S.; Sarma, D. D. *J. Phys. Chem. B* **2006**, *110*, 22310.
(20) Yang, Y.; Chen, O.; Angerhofer, A.; Cao, C. J. *J. Am. Chem. Soc.* **2006**, *128*, 12428.
(21) Pradhan, N.; Peng, X. *J. Am. Chem. Soc.* **2007**, *129*, 3339.
(22) Nag, A.; Sapra, S.; Nagamani, C.; Sharma, A.; Pradhan, N.; Bhat, S. V.; Sarma, D. D. *Chem. Mater.* **2007**, *19*, 3252.
(23) Lommens, N. P.; Loncke, F.; Smet, P. F.; Callens, F.; Poelman, D.; Vrielinck, H.; Hens, Z. *Chem. Mater.* **2007**, *19*, 5576.
(24) Archer, P. I.; Santangelo, S. A.; Gamelin, D. R. *Nano Lett.* **2007**, *7*, 1034.
(25) Nag, A.; Sarma, D. D. *J. Phys. Chem. C* **2007**, *111*, 13641.
(26) Thakar, R.; Chen, Y.; Snee, P. T. *Nano Lett.* **2007**, *7*, 3429.
(27) Huynh, W. U.; Dittmer, J. J.; Alivisatos, A. P. *Science* **2002**, *295*, 2425.

systems.[1] Strangely enough, however, it has proven persistently and frustratingly difficult to incorporate a sizable amount of manganese as well as other dopants into such nanocrystal hosts, in spite of high solubility of the dopant in the same bulk host. Two independent suggestions have been put forward in the literature to explain this baffling phenomenon.[16,17] In one,[17] it is suggested that the doped Mn^{2+} ion in such nanoclusters as CdSe is invariably in an energetically unfavorable state, preferring to be ejected to the surface of nanoclusters. Erwin et al.,[16] however, proposed that the ease of initial adsorption of impurities on specific surfaces of a growing nanocrystal kinetically controls the extent of impurity doping; specifically, Mn^{2+} ions get easily adsorbed on (001) facets of a zinc-blende (ZB) structure resulting in easier Mn^{2+} doping in ZB NCs compared to their wurtzite (WZ) counterpart. Obviously, the rejection of Mn^{2+} from the host nanocrystal within the first mechanism will be facilitated by an increase in the temperature, and indeed, it has been observed[12,22] that an increase in reaction temperature anneals out the Mn^{2+} impurities, a phenomenon known as self-annealing.[12,17] But restricting the synthesis temperature to lower values introduces a higher defect density in nanoparticles, thereby reducing the photoluminescence (PL) quantum efficiency (QE) drastically. There are only a few reports[15,16,20,28] of Mn^{2+} incorporation into II−VI semiconducting NCs employing high temperature (∼573 K) syntheses, namely two reports[15,28] of Mn^{2+}-doped ZnSe NCs, one[20] of CdS/ZnS core/shell NCs and one[16] of ZnSe/CdSe core/shell NCs; in all these cases the host NCs have a ZB structure, suggesting the validity of ref 16 that stressed the difficulty of doping the WZ structured CdSe NCs, having achieved a very poor (0.14%) extent of doping. Recently, Archer et al.[24] reported up to ∼1% Mn^{2+} doping in WZ CdSe NCs at a relatively lower (488 K) reaction temperature. Interestingly, none of the works has achieved any substantial extent of doping even for the ZB structure. There has been an attempt[29] to incorporate a large extent of Mn^{2+} ions in ZnO NCs, with the help of rare single molecular precursors containing a prebonded Mn−O complex and by carrying out a reaction at a somewhat lower temperature (453 K) giving a weak and broad emission spectrum dominated by surface states. Thus, we may summarize the present empirical wisdom in the community as (1) it is difficult to dope Mn^{2+} in usual II−VI semiconductors in the nanometric (≤6 nm) regime beyond 1−2%; (2) it is considerably more difficult to dope a WZ system compared to the ZB ones; and (3) a relatively higher level of doping may be achieved with a lower reaction temperature, typically less than 470 K, this unfortunately leading to poor PL properties. Besides the fundamentally diverging suggestions[16,17] to explain the difficulty doping manganese into semiconducting NCs, the general inability to do so is worrisome in view of the immense technological importance of such doped systems, therefore requiring a critical investigation of this aspect.

Here we report the results of incorporating *high* concentrations (up to 7.5%) of manganese in *wurtzite* $Zn_xCd_{1-x}S$ NCs (size ∼6.5 nm) via a *high temperature* (∼583 K) synthetic route, forming a stable state unlike all previous suggestions and, at the same time, suggesting an intuitively appealing explanation for the past difficulties in achieving such doping. The underlying hypothesis of our approach is that the difficulty arises from the ionic size (Table S1, in Supporting Information) mismatch between the substituent dopant and the substituted cation, which would cause a significant amount of strain in the NC lattice; since strain fields are necessarily long range, much longer than typical NC dimensions, it tends to relieve itself by ejecting the dopant to the surface of NCs. Since lattice parameters of MnS lie between those of CdS and ZnS, tuning the average lattice parameters of the host NC, which in turn tune the void size available for dopant incorporation, by forming $Zn_xCd_{1-x}S$ NCs with different values of "x" provides an interesting way to verify/falsify this conjecture. Our results clearly show that minimization of the lattice mismatch of MnS with a $Zn_xCd_{1-x}S$ host lattice allows a substantially larger amount of manganese incorporation in the host lattice in spite of the WZ rather than the ZB structure of the synthesized NCs. Thus, we conclude that the lattice mismatch between the MnS and host lattice is the dominant factor determining the extent of Mn^{2+}-doping in such NCs, rather than the crystal structure[16] or the thermal factor.[12,17] En route, we have also achieved a high PL efficiency (∼25%), which may be further enhanced by fine-tuning the synthesis parameters.

Experimental Section

For a typical synthesis of $Zn_{0.49}Cd_{0.51}S$ NCs, the reaction mixture consisting of 0.386 mmol of CdO (s.d. fine-chemicals Limited), 0.330 mmol of ZnO (Leo Chemical), 1 mL of oleic acid (Loba Chemie), and 10 mL of 1-octadecene (Aldrich) was degassed with argon at 413 K for 30 min. It was then heated up to 583 K giving a clear solution, which is then cooled to 578 K. Oleyl amine (Aldrich, 1 mL) was injected to the above solution resulting in an ∼5 K drop in temperature. The reaction mixture is then reheated to 578 K within 20 s, and a solution of S (1.9 mmol in 1 mL of 1-octadecene) is injected followed by growth at 583 K for 20 min. All the steps have been carried out in an argon atmosphere, and the product NCs were precipitated and washed repeatedly with 1-butanol. $Zn_xCd_{1-x}S$ nanocrystalline samples were prepared using precursor concentration ratios in the reaction with $x = 0$, 0.28, 0.46, 0.61, and 1. Elemental compositions of the product NCs obtained by inductively coupled plasma atomic emission spectroscopy (ICP-AES) using a Perkin-Elmer's Optima 2100 DV spectrometer shows $x = 0.32$, 0.49, and 0.63, in close agreement with the precursor concentration ratios in the reaction mixture corresponding to $x = 0.28$, 0.46, and 0.61, respectively. To prepare Mn^{2+}-doped $Zn_xCd_{1-x}S$ NCs, thus giving a composition of $(Zn_xCd_{1-x})_{1-y}Mn_yS$, a solution of $Mn(CH_3COO)_2 \cdot 4H_2O$ (Merck) in oleyl amine is added, instead of only oleyl amine, keeping all other steps exactly the same as those for undoped samples. Oleyl amine is mainly used as a solvent for the Mn^{2+} precursor; however, it also helps to achieve uniform spherical particles.

Transmission Electron Microscopy (TEM) data were obtained using a JEM 2010 HRTEM, JEOL microscope at an accelerating voltage of 200 kV. Powder X-ray diffraction (XRD) patterns were recorded on a Siemens D5005 diffractometer using Cu Kα radiation. All the PL spectra were measured by using a Perkin-Elmer LS 55 Luminescent spectrometer after dispersing the NCs in toluene. The PL QE was measured using fluorecein as the reference dye for the Mn^{2+} d emission.

Results and Discussion

Figure 1a shows Powder XRD patterns for NCs of $Zn_xCd_{1-x}S$ with $x = 0$, 0.32, 0.49, and 0.63, establishing a WZ crystal structure for all, as evident from a comparison with standard (ICSD) WZ patterns for bulk CdS, MnS, and ZnS. However,

(28) Norris, D. J.; Yao, N.; Charnock, F. T.; Kennedy, T. A. *Nano Lett.* **2001**, *1*, 3.
(29) Wang, Y. S.; Thomas, P. J.; O'Brien, P. *J. Phys. Chem. B* **2006**, *110*, 21412.

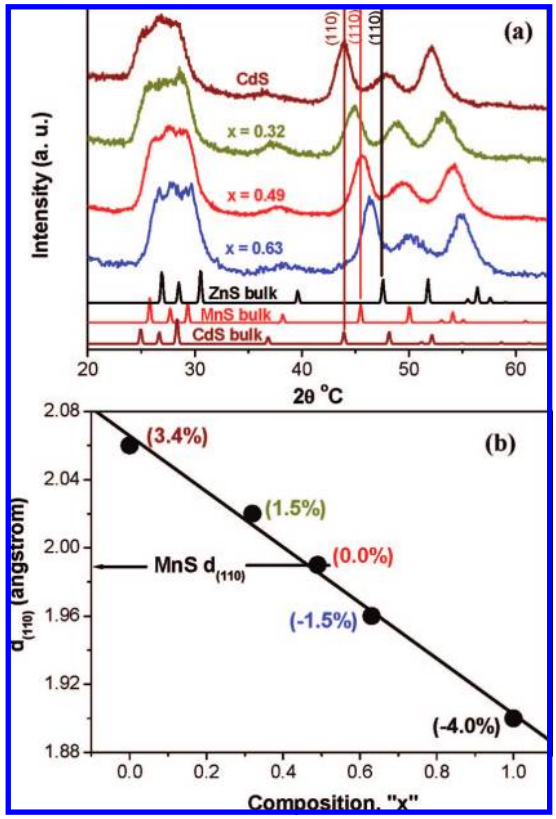

Figure 1. (a) X-ray diffraction patterns for $Zn_xCd_{1-x}S$ NCs with different values of "x". Reference XRD pattern for wurtzite structure of bulk CdS, MnS, and ZnS are taken from ICSD. (b) The plot of the interplanar distance ($d_{(110)}$) for (110) plane of $Zn_xCd_{1-x}S$ NCs as a function of composition, x, exhibiting a linear dependence in accordance with Vegard's Law of alloy formation; $d_{(110)}$ value for $x = 1$ is taken from the standard wurtzite pattern of bulk ZnS. The lattice mismatch of MnS with $Zn_xCd_{1-x}S$ for different x values is shown in parentheses.

ZnS NCs synthesized with identical reaction conditions exhibit a characteristic ZB structure, shown in Figure S1 of the Supporting Information. XRD peaks in Figure 1a shift continuously to larger angles with an increase in zinc content, suggesting an alloy formation. Figure 1b shows a linear dependence of the interplanar distance ($d_{(110)}$) for (110) planes for these NCs with composition x, which confirms[30,31] the formation of the $Zn_xCd_{1-x}S$ alloy following Vegard's Law and rules out the possibility of core/shell structures as well as a separate nucleation of CdS and ZnS NCs. This is also suggested by the optical absorption (Figure S2 of the Supporting Information) and emission (not shown here) spectra of these NCs exhibiting a single bandgap feature that moves systematically to higher energies with increasing zinc concentration. The lattice mismatch of MnS with $Zn_xCd_{1-x}S$ for different x values was calculated from the corresponding $d_{(110)}$ using the equation

$$\%\ \text{lattice mismatch} = 100 \times \left(d^{\text{host}}_{\langle 110\rangle} - d^{\text{MnS}}_{\langle 110\rangle}\right) / d^{\text{host}}_{\langle 110\rangle}$$

and are shown in parentheses in Figure 1b; the arrow indicates the $d_{(110)}$ for bulk MnS, suggesting near identical lattice parameters with $Zn_{0.49}Cd_{0.51}S$ NCs.

Figure 2a shows the TEM image for the synthesized $Zn_{0.49}Cd_{0.51}S$ NCs doped with 0.9% manganese. All samples

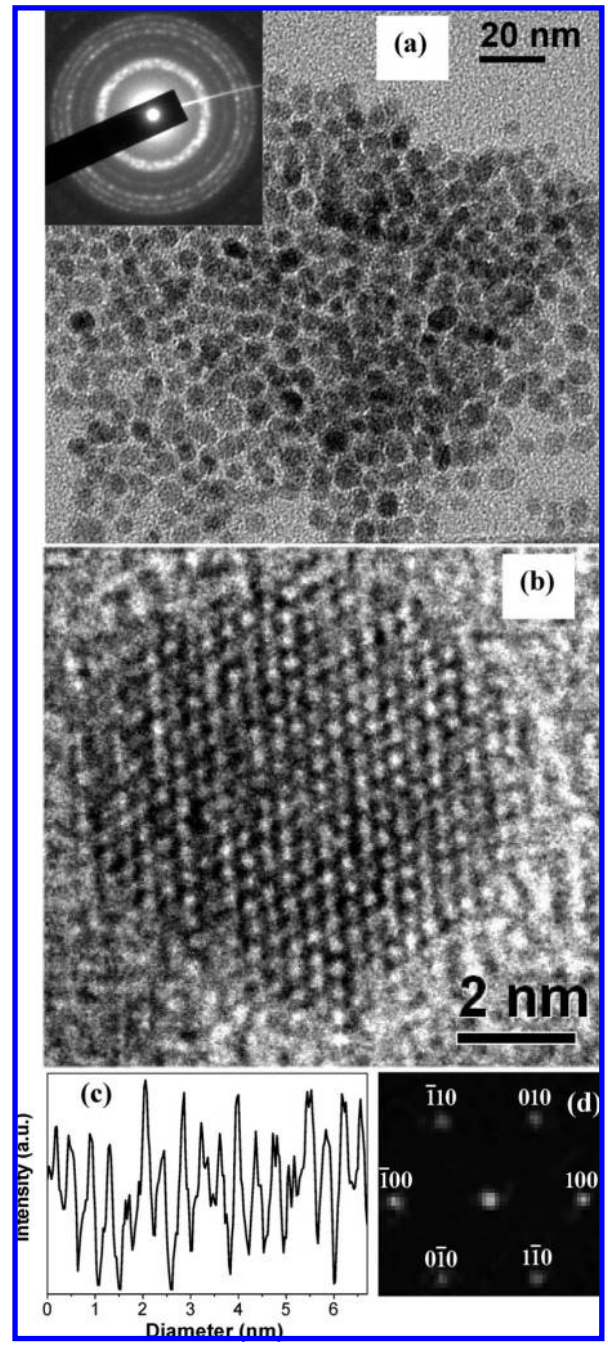

Figure 2. TEM images (a) and (b) with different magnification for 0.9% Mn^{2+}-doped $Zn_{0.49}Cd_{0.51}S$ NCs. Inset to Figure 2a shows the selected area electron diffraction pattern of the sample. (c) Intensity line profile of the bright and dark spots along a lattice plane taken from Figure 2b. (d) FFT of the image shown in Figure 2b.

across the different compositions of $Zn_xCd_{1-x}S$ NCs show TEM images with similar average diameters. Nearly spherical particles with an average diameter of 6.5 nm and 8.5% size distribution are observed. The inset shows the selected area electron diffraction pattern characteristic of a wurtzite phase. One representative High Resolution TEM (HRTEM) phase contrast image of a single particle of the sample is shown in Figure 2b. Continuous lattice fringes throughout the whole particle reveal the single crystalline nature of the nanocrystal without any observable defect. Contrast of HRTEM depends on the electron scattering;[32] thus, for similar lattice parameters, ZnS is expected to exhibit lower contrast compared to CdS, since it has fewer

(30) Zhong, X.; Han, M.; Dong, Z.; White, T. J.; Knoll, W. *J. Am. Chem. Soc.* **2003**, *125*, 8589.
(31) Zhong, X.; Feng, Y.; Knoll, W.; Han, M. *J. Am. Chem. Soc.* **2003**, *125*, 13559.

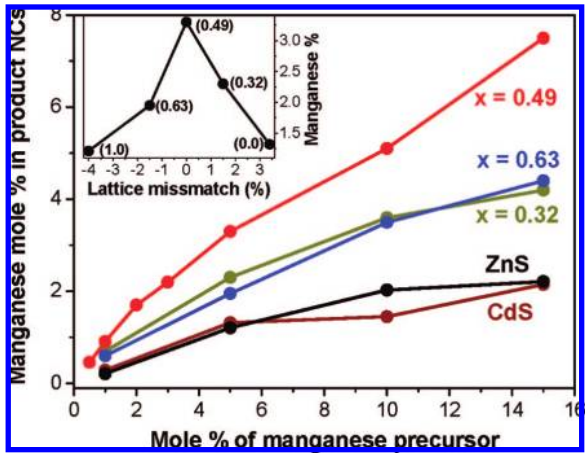

Figure 3. Manganese mole percent in the synthesized NCs measured by ICP-AES as a function of that in the reaction mixture for various compositions of NCs. The inset shows the dependence of manganese concentration doped in NCs as a function of the lattice mismatch between MnS and $Zn_xCd_{1-x}S$ NCs for a given (5%) precursor concentration of manganese; the values of corresponding "x" are shown in parentheses.

electrons per unit cell. Figure 2c shows the intensity line profile along a lattice plane taken from Figure 2b, where bright and dark spots in Figure 2b correspond to the peak and dip in intensity, respectively, in Figure 2c. The difference in intensity between the adjacent peak and dip represents the contrast. We do not observe any stepwise change in the contrast across the diameter of the nanocrystal; this suggests a random distribution of cations, instead of any heterostructured nanocrystal or a phase separation within the single nanocrystal, providing additional support to the conclusions based on XRD results. The interplanar distance calculated from the HRTEM image is 3.44 Å, which is in between those for (100) planes for the WZ phase of bulk CdS (3.58 Å) and ZnS (3.32 Å) but matches with that of bulk MnS (3.45 Å). Figure 2d shows a Fast Fourier Transform (FFT) of the image shown in Figure 2b. A perfect hexagonal pattern with equidistant dots from the zone axis and an angle of 60° between any two adjacent dots through the zone axis is obtained. This pattern along with the observed interplanar distance in Figure 2b confirms[33] the WZ structure of the synthesized NCs, and the lattice fringes in Figure 2b correspond to (100) planes with zone axis [001]. For a homogeneous $Zn_xCd_{1-x}S$ alloy, lattice parameters vary[31] linearly with "x", and a comparison of the obtained $d_{(110)} = 3.44$ Å with those of CdS and ZnS gives $x = 0.54$, which is essentially the same as that ($x = 0.49$) obtained by ICP-AES within experimental uncertainties, establishing the internal consistency between independent measurements.

In order to probe our ability to dope such alloy NCs within a high temperature synthesis and in spite of the NCs being in the WZ structure, we carried out the synthesis in the presence of varying amounts of Mn^{2+} precursors in the reaction mixture for every composition of the alloy NC. The XRD patterns of the Mn^{2+} doped and undoped $Zn_xCd_{1-x}S$ for a given "x" are almost identical (Figure S3 of Supporting Information) suggesting independence of the NC size and crystal structure on the manganese content. Figure 3 shows the mole percentage of manganese in product NCs obtained by ICP-AES with respect to the mole percentage of the manganese precursor used during the synthesis of Mn^{2+}-doped $Zn_xCd_{1-x}S$ samples with different values of x. These results show the expected increase in the incorporation of manganese in NCs of all compositions with increasing Mn^{2+} precursor concentration; however, it is clear from the plots that manganese incorporation remains consistently low (<2%) for pure CdS and ZnS NCs. In passing, we also note that the CdS NC has the WZ structure in contrast to the ZB structure of ZnS NCs, while the extent of manganese incorporation is very similar for both systems at all precursor concentrations, indicating structural considerations, suggested earlier,[16] being relatively less important in determining the extent of manganese incorporation. Interestingly, these results establish a very pronounced dependence of the extent of manganese doping on the nanocrystal composition, x. We illustrate this more clearly in the inset to Figure 3 which shows the manganese content at a given manganese precursor concentration (5 mol %) as a function of the lattice mismatch (bottom axis), with the composition (x) shown in parentheses. There is an evident maximum of manganese content for $Zn_xCd_{1-x}S$ NCs with $x = 0.49$ that has no lattice mismatch with MnS, and the manganese content decreases systematically with increasing compressive as well as tensile lattice mismatches; the same behavior is found for all manganese precursor concentrations, as is evident from the main part of Figure 3. This systematic trend cannot be explained, if we consider that the major amount of manganese is present only in the surface of these NCs or in surroundings, suggesting that the major amount of manganese is indeed incorporated in the host lattice. Unfortunately, such a high concentration of manganese incorporation into the lattice of the NC cannot be established using a standard technique, such as Electron Paramagnetic Resonance (EPR) spectroscopy in contrast to its efficacy at low dopant concentrations. At low concentrations of Mn^{2+}, EPR clearly shows the hyperfine lines corresponding to tetrahedral Mn^{2+} ions incorporated into the bulk, distinguishing such doped ions from the surface species; such EPR spectra (not shown here) are indeed observed in our samples for low doping of Mn^{2+}. However, the EPR spectra from samples with higher doping levels become broad and featureless due to dipolar interactions. This restricts the applicability of the EPR technique to probe the higher level of doping achieved here. Instead, we made indirect approaches to confirm that a large amount of manganese indeed becomes incorporated in the host lattice. NCs were extracted after different growth periods from a given reaction mixture and washed thoroughly with 1-butanol, as described before. We show typical TEM images from samples extracted after 5 and 1800 s of reaction time in Figure S4, of the Supporting Information. These samples are found to have average diameters of 2.8 and 6.3 nm, respectively, suggesting significant growth over this period of time. We estimated the manganese concentration in these two samples to be 4.6% and 7.5%, respectively. These results strongly suggest incorporation of manganese into the growing NC throughout the growth period, indicating a nearly homogeneous incorporation of manganese. The slight, but steady, increase of manganese concentration with the growth time is attributed to an increasing doping efficiency with the size of the nanoclusters. In passing, we note that the Zn/Cd ratio obtained from ICP-AES remains nearly constant throughout the growth process, supporting the idea of a homogeneous alloy formation of the host NCs. In order to address this issue of manganese incorporation in the bulk of NCs *vis-a-vis* on the surface, we etched the fully grown NCs obtained after 30 min of reaction time, corresponding to those in Figure 3, using

(32) Peng, X.; Schlamp, M. C.; Kadavanich, A. V.; Alivisatos, A. P. *J. Am. Chem. Soc.* **1997**, *119*, 7019.
(33) Williams, D. B.; Carter, C. B. *Transmission Electron Microscopy, A Textbook for Materials Science*; Plenum Press: New York, 1996.

benzoyl peroxide following the established[34] procedure. This procedure resulted in a decrease of the average particle size by about 0.8 nm, as confirmed by TEM images shown in Figure S4. This process of etching is expected to remove all of the manganese sticking to the surface along with some manganese also from the subsurface region. We reestimated the manganese concentration using ICP-AES for each sample with varying alloy compositions and different manganese precursor concentrations after such etching followed by a thorough washing. The process of etching leads to a decrease of the manganese concentration by about 20−40%. This decrease in the manganese concentration after etching can be a result of three possible reasons: (1) a fraction of the total manganese concentration is not incorporated in the lattice and remains on the surface of the NC; (2) inhomogeneous doping, with a higher dopant concentration in the subsurface region compared to that in the interior of the NC; and (3) a preferential etching of manganese. However, these experiments clearly establish that a substantial extent of manganese is indeed doped in the interior of the NC rather than being in the surface or subsurface regions. Even more importantly, we find that the manganese concentration in these etched samples follows exactly the same dependence of manganese concentration on the composition of the host NC, as shown in the inset of Figure 3, exhibiting a drastic maximum for the composition $Zn_{0.49}Cd_{0.51}S$ host NC with the least lattice mismatch with respect to MnS. This establishes the conclusion that the extent of manganese doping in the bulk of NCs can be tuned by tuning the lattice parameter of the host.

While the above experimental evidence for the dependence of manganese concentration on the average lattice parameter is conclusive, a microscopic description for the origin of this effect is less obvious at this stage. The intuitively appealing argument based on tuning the lattice parameter to match that of the dopant has obvious limitations to explain this phenomenon from a microscopic point of view. The observed lattice parameter from XRD peak positions is averaged information over the randomly substituted alloy, where in reality a bimodal distribution of bond lengths arising from $Zn^{2+}-S^{2-}$ and $Cd^{2+}-S^{2-}$ bonds is expected, as shown in ref 35 with an example of $Cd_{1-x}Zn_xSe$ NCs. Our preliminary Extended X-ray Absorption Fine Structure (EXAFS) investigations[36] of the present $Zn_xCd_{1-x}S$ samples confirm this expectation. Thus, the alloy cannot be thought naively to have the average bond length for both of these cation−anion bonds (Zn^{2+}/$Cd^{2+}-S^{2-}$), where manganese is incorporated efficiently with a matching of $Mn^{2+}-S^{2-}$ bond length with the common Zn^{2+}/$Cd^{2+}-S^{2-}$ bond length. We believe that a better microscopic description of Mn^{2+} incorporation can be provided schematically as shown in Figure 4 in terms of a highly simplified, two-dimensional analogue of a local description of the alloy formation between ZnS and CdS around a cationic vacancy. The left figure illustrates a local description of a cation (Zn^{2+}) vacancy at the center of the square formed by the nearest neighbor $Zn^{2+}-S^{2-}$ bonds. Mn^{2+} is supposed to occupy the cationic vacancy site, which becomes difficult due to the small volume associated with Zn^{2+} vacancy. Mn^{2+} at the center of the square would cause compressive strain on neighboring bonds by effectively expanding the square. The opposite will happen when the size of the cationic vacancy is larger than the dopant ion, as illustrated schematically with the figure on the right representing the case of CdS. This situation

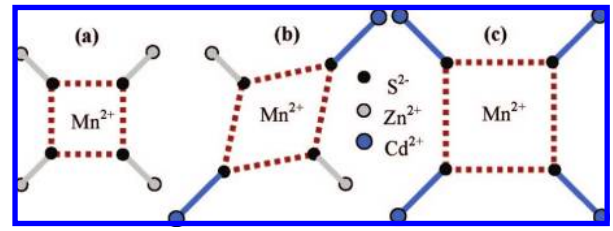

Figure 4. Simplistic two-dimensional cartoon comparing the size of the cationic vacancy available for Mn^{2+} incorporation in (a) ZnS, (b) $Zn_{0.5}Cd_{0.5}S$, and (c) CdS lattice. While circles and solid lines represent corresponding ions and bond lengths, respectively, the areas covered by the dotted lines reflect the size of the cationic vacancy in each of the three host lattice.

is expected to lead to a tensile strain on the surrounding of the doped Mn^{2+} site. Thus, it appears reasonable that the volume available to dope Mn^{2+} may be optimized by tuning the composition of the alloy, as illustrated in the middle panel in Figure 4. While this oversimplified schematic description neither includes the proper bond angles of the sp^3 hybridization, representing the three-dimensional tetrahedral void as a two-dimensional, square one, nor shows all the bonds of the first and second nearest neighbors and, therefore, is inaccurate in many details, it is still useful to point out the trend in size of the cationic vacancy available for Mn^{2+} incorporation with a change in composition of the host NC.

We have confirmed that the maximal incorporation of manganese in $Zn_xCd_{1-x}S$ NCs for $x = 0.49$ is not a kinetically trapped metastable state reached accidentally by annealing the sample dispersed in 1-octadecene at 573 K, limited by the boiling point of the solvent, for a long period of time (∼5 h), followed by a thorough washing of the sample and then re-estimating of the manganese content; no change in manganese concentration was found even after such a prolonged heating. A recent report[35] of doping Co^{2+} in ZnSe and CdSe can also be related to our results. It was shown that Co^{2+} doping is more facile in ZnSe compared to CdSe, explained in terms of a substantially larger mismatch of the $Co^{2+}-Se^{2-}$ bond length with that of $Cd^{2+}-Se^{2-}$ as compared to $Zn^{2+}-Se^{2-}$. This work[35] also concluded that Mn^{2+} doping in CdSe and ZnSe introduced similar lattice strain because of the equally large mismatch of the $Mn^{2+}-Se^{2-}$ bond length with those of $Cd^{2+}-Se^{2-}$ and $Zn^{2+}-Se^{2-}$, the optimal $Mn^{2+}-Se^{2-}$ bond length falling midway between these two limits. These conclusions agree well with the difficulty of doping Mn^{2+} in ZnS and CdS NCs but the greater ease of doping $Zn_xCd_{1-x}S$ alloy NCs found in the present results.

These nanoparticles exhibit interesting photophysical properties, besides achieving a high PL QE. We discuss these results with respect to the optimal composition of $Zn_{0.49}Cd_{0.51}S$ as a function of manganese doping as a representative case. We show PL spectra normalized by their corresponding absorbances at the excitation wavelength in the inset to Figure 5, exhibiting the sharp band gap emission at ∼444 nm and the Mn^{2+} emission at ∼585 nm. The small random variation in peak position of the band gap emission is because of experimental uncertainties in terms of composition and size of the synthesized NCs. A small but systematic red shift in the Mn^{2+} emission peak position from 584 to 589 nm was observed with an increase in manganese concentration from 0.5% to 7.5%; such a shift has

(34) Battaglia, D.; Blackman, B.; Peng, X. *J. Am. Chem. Soc.* **2005**, *127*, 10889.
(35) Santangelo, S. A.; Hinds, E. A.; Vlaskin, V. A.; Archer, P. I.; Gamelin, D. R. *J. Am. Chem. Soc.* **2007**, *129*, 3973.
(36) To be published.

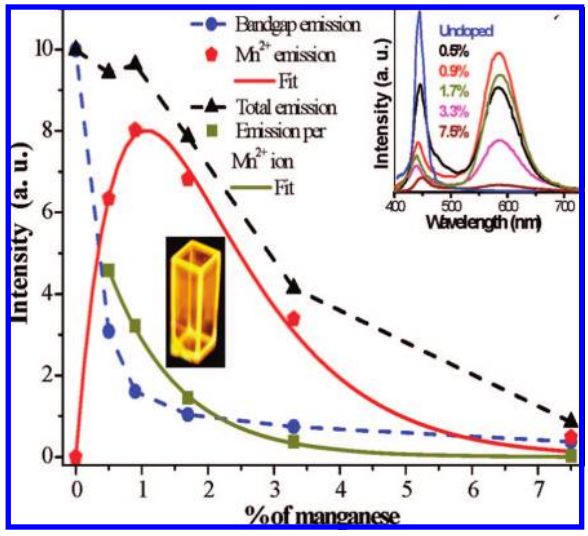

Figure 5. Variations of intensities for bandgap emission, Mn^{2+} d-emission, total PL emission, and Mn^{2+} d-emission per Mn^{2+} ion as a function of the manganese concentration in $Zn_{0.49}Cd_{0.51}S$ NCs. These data were derived from the corresponding PL spectra, normalized by the corresponding absorbance at the excitation wavelength (385 nm), as shown in the inset; the emission spectrum for the undoped sample was divided by three for a better representation. The calculated best fits, dark-yellow and red solid lines, to Mn^{2+} d-emission per Mn^{2+} ion and total Mn^{2+} emission, respectively, are superimposed on experimental data points for comparison. Mn^{2+} d-emission intensities per Mn^{2+} ion and the corresponding fitting curve were multiplied by 13 to plot it within the same scale. Photographs of emission of empty cuvette that had the solution of 0.9% Mn^{2+}-doped $Zn_{0.49}Cd_{0.51}S$ NCs, after excitation at 365 nm using a custom-made UV-source used for thin layer chromatography. Trace amount of sample sticking to the empty cuvette wall was found sufficient to provide a bright glow.

been earlier attributed[37] to the larger contribution to the emission spectrum from exchanged couple Mn^{2+} pairs. The spectra show a nonmonotonic dependence of Mn^{2+} emission with the maximum intensity for 0.9% manganese, while the band gap emission monotonically decreases with manganese doping. Separating the contributions from the band gap emission and the manganese emission and integrating over their spectral ranges, we obtain the absorption-normalized emission intensities from these two types of de-excitation for these samples. The absorbance-normalized total (band gap + Mn^{2+}) emission intensity, band gap emission intensity, Mn^{2+}-related emission intensity, and Mn^{2+} emission intensity per Mn^{2+} ion are shown in the mainframe of Figure 5, also tabulated in Table S2 of the Supporting Information. Interestingly, the band gap emission (blue circles) drops precipitously for small manganese dopings up to ~1%; simultaneously, the Mn^{2+} emission intensity (red pentagons) increases rapidly, thereby maintaining the total emission intensity (black triangles) at about the same level. This clearly suggests an energy transfer from the nanocrystal host to the doped sites with nearly ideal efficiency. Beyond ~1%, the total emission intensity decreases rapidly with increasing manganese content, driven primarily by a rapid drop in the total Mn^{2+} emission intensity (red pentagons). The cause of this rapid drop in the total Mn^{2+} emission intensity can be understood by monitoring the Mn^{2+} emission intensity *per* Mn^{2+} ion (dark-yellow squares), obtained by dividing the total intensity by the manganese concentration in each case; evidently there is a rapid decrease of the emission intensity per Mn^{2+} ion with increasing manganese content, arising from a PL quenching due to $Mn^{2+}-Mn^{2+}$ interactions. Thus, the QE for PL from individual Mn^{2+} ions is the highest for the most dilute limit. However, the total Mn^{2+} PL efficiency, being a product of manganese content and the PL efficiency for each Mn^{2+} ion, is optimized at a finite, intermediate manganese content.

In the absence of the availability of any microscopic theory, we have fitted the rapidly decreasing Mn^{2+} emission intensity per Mn^{2+} ion as a function of the manganese content with different analytical forms, such as algebraic and exponential forms. It is found that the dependency is best described by a single exponential decay as shown by the dark-yellow calculated line in Figure 5, showing a remarkable agreement with experimental data points. While the origin of this very interesting dependence requires further investigation, such a study is clearly beyond the scope of the present work. However, multiplying the best-fit exponential function describing the individual Mn^{2+}-ion quantum efficiency with the manganese content, we obtain a prediction for the nonmonotonic dependence of the total Mn^{2+} emission from these NCs as a function of the manganese content. This analytical expression *without any adjustable parameter* is plotted in Figure 5 with the red solid line, in surprising agreement with experimental points (red pentagons) providing further credence to the present analysis. We estimated the quantum efficiency of total emission to be ~25% for samples with up to ~1% manganese with a rapid decrease for higher manganese content. Figure 5 contains a photograph of the glowing empty cuvette obtained after pouring out a solution of a 0.9% Mn^{2+}-doped $Zn_{0.49}Cd_{0.51}S$ nanocrystal sample under irradiation from a simple UV source normally used for thin layer chromatography; a trace amount of the sample sticking on the inner surface of the empty cuvette is sufficient to cause a significantly intense yellow glow easily visible to the naked eye.

Conclusions

We have experimentally established that the vexing problem encountered in attempts to dope semiconducting NCs with transition metal ions, such as Mn^{2+}, is caused primarily by the mismatch between the space required to accommodate the dopant ion and the space associated with the cationic site of the semiconducting host, usually making a metastable or an unstable state. By adjusting the average lattice parameter of the host semiconducting cluster by tuning its composition, the space available for a dopant substitution at the cationic site can be optimized, thereby allowing us to incorporate to a much larger extent manganese than was achieved earlier within a high temperature synthesis and for a crystal structure, namely wurtzite, so far believed to be detrimental to manganese doping; this proves that the perceived metastability of the doped state is not inevitable. The high temperature synthesis, as a byproduct, leads to a very high PL efficiency. The optimum manganese content for maximizing PL efficiency is determined by a competition between two opposite trends, namely the number of dopant ions and the quantum efficiency of each dopant ion. We find the striking experimental fact that the quantum efficiency per Mn^{2+} ion in the nanocrystal decreases exponentially with the average number of dopants per nanocrystal. These results, establishing a general route to doping a large range of transition metal ions in semiconducting nanocrystal hosts, is expected to have important consequences also in the field of nanospintronics materials such as nano-DMS materials, which are known to be plagued by concerns of impurity phases and precipitates involving dopant ions.

(37) Suyver, J. F.; Wuister, S. F.; Kelly, J. J.; Meijerink, A. *Phys. Chem. Chem. Phys.* **2000**, *2*, 5445.

Acknowledgment. Authors acknowledge Department of Science and Technology and Board of Research in Nuclear Sciences, Government of India, for funding the project. D.D.S. acknowledges the National J. C. Bose Fellowship. A.N. acknowledges CSIR, Government of India for a fellowship.

Supporting Information Available: Ionic radii table; XRD patterns for ZnS and $Zn_{0.49}Cd_{0.51}S$ NCs doped with various amounts of Mn^{2+}; UV−visible absorption spectra for $Zn_xCd_{1-x}S$ NCs; TEM images of the NCs from the aliquots taken after 5 s, 1800 s, and the etching experiment; and a table containing data relevant to the photophysical study.This material is available free of charge via the Internet at http://pubs.acs.org.

JA801249Z